*J. Fluid Mech.* (1992), *vol.* 241, *pp.* 443–467
*Printed in Great Britain*



# On turbulent separation in the flow past a bluff body

By A. NEISH AND F. T. SMITH
Department of Mathematics, University College London, Gower Street, London WC1E 6BT, UK

(Received 14 February 1990 and in revised form 16 January 1992)

The basic model problem of separation as predicted by the time-mean boundary-layer equations is studied, with the Cebeci–Smith model for turbulent stresses. The changes between laminar and turbulent flow are investigated by means of a turbulence 'factor' which increases from zero for laminar flow to unity for the fully turbulent regime. With an attached-flow starting point, a small increase in the turbulence factor above zero is found to drive the separation singularity towards the trailing edge or rear stagnation point for flow past a circular cylinder, according to both computations and analysis. A separated-flow starting point is found to produce analogous behaviour for the separation point. These findings lead to the suggestion that large-scale separation need not occur at all in the fully turbulent regime at sufficiently high Reynolds number; instead, separation is of small scale, confined near the trailing edge. Comments on the generality of this suggestion are presented, along with some supporting evidence from other computations. Further, the small scale involved theoretically has values which seem reasonable in practical terms.

## 1. Introduction

Turbulent separating flows in practice tend to be highly unsteady (see e.g. Bogdonoff 1987), with the flow at any point changing rapidly, and by significant amounts, from one instant to the next. Despite the resulting doubts on the relevance of time-mean quantities, turbulent boundary layers are nevertheless broadly accepted to be less prone to separate than the corresponding laminar ones, owing to the enhanced wall shear stresses generally. Here, to help quantify that further, and given the limited extent of analysis so far, we take the time-mean equations and examine the flow processes involved near separation, using a particular basic closure model and assuming the turbulent boundary layer to be fully developed upstream. Also, the ensemble-averaged flow is modelled as planar and steady, for an incompressible fluid, so that the essential features can be explored.

Experimental measurements of turbulent separation are understandably difficult to make, especially within the short scales near separation, owing to the unsteadiness above, hindering precise measurements of time-mean quantities. One study to note for an extensive investigation of larger-scale properties is by Patrick (1985), concerning turbulent separation and reattachment on a flat plate. Other experiments on the character of turbulent separation include those of Simpson, Strickland & Barr (1977) and Simpson, Chew & Shivaprasad (1981), which suggest that logarithmic layers are absent at the mean-flow separation; see also Stratford (1959) and the present work below. Thompson & Whitelaw (1985) show the importance also of

normal stresses there. Other works include Achenbach (1971), on the flow past rough circular cylinders, and Trupp, Azad & Kassab (1986), Dengel & Fernholz (1990).

On the theoretical side, for the attached unperturbed turbulent boundary layer, Mellor (1972), Bush & Fendell (1972) and Fendell (1972) consider the asymptotic structure at large Reynolds numbers $Re$, using a general form for the turbulence closure consistent with a two-tiered boundary layer. Deriat & Guiraud (1986) study the asymptotics of turbulence in a boundary-layer structure and make some interesting remarks on the suitability of specific turbulence-closure models. The two-tiered work is followed and extended significantly by Melnik and his co-workers (Melnik, Chow & Mead 1977; Melnik 1980, 1987; Melnik & Grossman 1982) for the examination of trailing-edge motions, transonic conditions and interactive effects, the latter also being studied by Sykes (1980). Flow in the boundary layer's inner tier, including time-dependence, is investigated by Walker & Abbott (1977), Walker & Scharnhorst (1977), and Walker, Scharnhorst & Weigand (1986), the first in particular emphasizing the necessity of understanding theoretically the two-dimensional time-mean case in order to provide a basis for more complex flows. Proposals for the structure of turbulent separation are put forward by Sychev & Sychev (1980) and Sychev (1987) and are discussed later in this paper. Again, a family of velocity profiles for separated flows is suggested by Lock (1987), using various shape factors. Some more general ideas regarding the importance of the details of the turbulence closure model in asymptotic analysis are given by Gersten (1987), including the suggestion that the effects of such specific details on the main flow properties are secondary (see also our views below). Of interest as regards linear analysis in stratified turbulent flow are papers by Hunt, Leibovich & Richards (1988), Hunt & Richards (1984). (In anticipation of what follows, and prompted by a comment from J. C. R. Hunt, we note that linear analysis and the current nonlinear theory agree that the phase of the surface shear stress tends to that of the external *pressure* or mean flow in turbulent boundary layers as opposed to being controlled by the *pressure gradient* in laminar layers; see Ackenbach's 1971 experiments.) In work related a little to the present study, the trailing-edge and wake flow is considered theoretically by Alber (1980), Bogucz & Walker (1987) and Neish & Smith (1988), the latter's predictions comparing well with experiments and computations.

Computationally, there have been many attempts at comparing various closure models, e.g. zero- and two-equation, by computing flow solutions using each in turn and comparing the results; see e.g. Johnson & King (1985), Escande & Cambier (1985), Degrez & Vandromme (1985). The comparisons are mixed, producing no firm general conclusions. There appear to be few studies for the separation case and the effects of increasing turbulence factor in the boundary layer or indeed of the Reynolds number, apart from Barnett & Carter's (1986) Reynolds-number study for airfoils and bluff bodies using interactive boundary-layer theory. Flat-plate and wake flows are addressed numerically by Cebeci *et al.* (1979), among others, using a set of classical boundary-layer equations and the Cebeci–Smith (1974) turbulence model, modified for the wake part of the calculation. Other related studies of interest are by Inouye, Marvin & Sheaffer (1972), Cebeci, Stewartson & Whitelaw (1984), Bradshaw (1970), Andreopoulos & Bradshaw (1980), Chevray & Kovasznay (1969), Pot (1979), Ramaprian, Patel & Sastry (1982) and Hoffman & Ny (1978).

Concerning the development of a turbulent-separation theory, then, there appear to be few or no direct comparisons possible with either computation or experiment, as there are apparently little detailed data available. Only qualitative general

comparison can be made, such as the possible development of a Coles (1956) wake form in the velocity profile near separation and the movement of the separation point downstream with increasing Reynolds number (e.g. Barnett & Carter). The present theoretical study is therefore aimed at providing some comparisons, and questions, on the flow structure near separation, and yielding predictions, for comparisons with more comprehensive experimental and numerical studies, as regards Reynolds-number effects in particular.

This paper considers whether the choice of a specific representative turbulence model, in this case a relatively simple algebraic Cebeci–Smith model, may account adequately for a turbulent boundary layer as it approaches separation. There have been doubts that such a simple closure can describe separating flow with any physical validity, because the possibly new processes that govern the separation, involving turbulent kinetic energy production, may require severe modification of the turbulence closure model. (Similar doubts were considered, along with the eradication of the logarithmic layer, by Neish & Smith 1988 for wake flow.)

The fully turbulent separating-flow structure is tackled theoretically here by a gradual build-up from the laminar regime. A turbulence-level gauge factor $\bar{T}$ is brought into the Cebeci–Smith model (see (1.1) below), such that the flow can be varied continuously from the laminar to the fully turbulent state by increasing $\bar{T}$ from zero to one. With the attached-flow strategy adopted initially, the first significant range of $\bar{T}$ encountered is then of order $Re^{-\frac{1}{2}}$ since that first affects the classical boundary layer. The breakdown associated with the Goldstein (1948) singularity is found to be forced towards the trailing edge, from its original laminar position, as the parameter $Re^{\frac{1}{2}}\bar{T}$ is increased. This comes from computations on the circular-cylinder case (§2) and from analysis (§3) of the interesting multi-structured flow properties developing at large $Re^{\frac{1}{2}}\bar{T}$, the two approaches showing good agreement. The breakdown position approaches the trailing edge or rear stagnation point asymptotically, albeit in an approximately logarithmic fashion; and the boundary layer develops a two-tiered format, with its displacement thickness becoming singular at the onset of the trailing edge, prior to the breakdown. These findings lead on to the proposal in §5 for fully turbulent flow.

With a quite different, separated-flow strategy as the starting point instead (§4), a similar overall trend is observed as $\bar{T}$ is increased. The breakaway-separation position is found to be pushed downstream from the laminar-flow value, and the eddy size decreases, eventually producing a collapse around the trailing edge. This is due mainly to the enhancement of the wall shear stress just ahead of the separation process, as $\bar{T}$ increases.

The fully turbulent flow theory, and discussions, in §5, then take up the suggestions from §§2–4 (see also figure 1), with the parameter $\bar{T}$ increased to unity as required. The flow structure and scales are implied directly by those of §3 in fact, and over most of the body there is a standard, attached, two-tiered turbulent boundary layer. This is able to stay attached right from the leading edge to the verge of the trailing edge, even for a circular cylinder, because the Goldstein breakdown can no longer occur in that interval (cf. §3). The outer small-velocity-deficit tier thickens in singular fashion just prior to the trailing edge, such that a small non-slender zone of dimensions approximately $O(u_\tau^{\frac{1}{2}} l_D)$ is brought into operation locally. (Here $u_\tau$ is the non-dimensional friction velocity and $l_D$ is the global lengthscale, e.g. airfoil chord.) The flow there is controlled predominantly by a nonlinear balance between inertial, induced pressure-gradient, and turbulent-stress forces, the velocity deficit is no longer small, and so the modelling of all the turbulence stress terms

becomes crucial. In addition, an unknown slip velocity is thereby induced near the body surface (see also the Appendix), provoking a laminar–turbulent stress sublayer at the surface, and (as in §3) the logarithmic near-surface behaviour is eradicated locally. This structure, including embedded sublayers, is believed to control the final stages of any separation present. The separation eddy may be confined locally, or extend as a slender layer into the relatively thin wake, or indeed be completely absent; but the principal conclusion here is that large-scale separation need not occur at all (with this closure model and similar ones (see Neish 1988), at large Reynolds numbers (see also later)), since the majority of the motion can remain attached. Separation, if any, is forced by the external flow for example reaching a stagnation point or altering abruptly, rather than gently as in the laminar regime, and the typical streamline slopes involved near turbulent separation are $O(1)$. See also comments on numerical values in the last paragraph of this section.

The Cebeci–Smith model taken here is widely used and its governing equations may be written in non-dimensional form as

$$\frac{\partial u}{\partial x}+\frac{\partial \bar{v}}{\partial \bar{y}}=0, \tag{1.1a}$$

$$u\frac{\partial u}{\partial x}+\bar{v}\frac{\partial u}{\partial \bar{y}}=-\frac{\partial p}{\partial x}+t_x+Re^{-1}\frac{\partial^2 u}{\partial \bar{y}^2}, \tag{1.1b}$$

where

$$t_x \equiv \begin{cases} \bar{T}a_5\bar{\delta}\dfrac{\partial^2 u}{\partial \bar{y}^2} & \text{for} \quad \bar{y} > \bar{y}_1(x), \qquad (1.1c) \\ \bar{T}\dfrac{\partial}{\partial \bar{y}}\left[\bar{y}^2 B\left(\dfrac{\partial u}{\partial \bar{y}}\right)^2\right] & \text{for} \quad 0 \leqslant \bar{y} < \bar{y}_1(x). \qquad (1.1d) \end{cases}$$

The constant $a_5$ $(= a_3 a_1^{-1}) = 0.105$, after the transformation in Neish & Smith to absorb the usual constants $a_1 = 0.16$, $a_2 = 26$, $a_3 = 0.0168$, and in general the junction $\bar{y}_1(x)$ is to be determined from the conditions of continuity of the velocity, the shear and the eddy viscosity. A slenderness version is used at this stage (cf. §5), so that $\partial p/\partial \bar{y} = 0$ in effect, and $\bar{\delta} = u_e \delta$ where

$$\delta = \int_0^\infty (1-u/u_e)\,\mathrm{d}\bar{y}$$

is the unknown displacement thickness. Also, $B = 1-\exp(-a_6 Re\, u_\tau \bar{y})$ where $a_6 (= a_2^{-1}a_1^{-\frac{1}{2}}) = 0.096\,15$. The coordinates $x, \bar{y}$ are tangential and normal to the body surface in turn, the corresponding velocity components are $u, \bar{v}$, the pressure is $p$, and the airfoil chord (or cylinder radius) and the free-stream speed are both unity, in the present non-dimensional terms. The parameter $\bar{T}$ introduced is unity in the fully turbulent modelled flow and zero for laminar motion, while in §§2, 3 we set $\bar{T} = Re^{-\frac{1}{2}}T$ initially. Many other developed closure models, we note, are similar to the Cebeci–Smith one (see the discussion in Neish 1988), and hence the conclusion at the end of the previous paragraph applies equally well to them.

Given that conclusion, it might well be argued that the major deficiency in the whole subject is still the ignorance over a closure model relevant during separation. (A referee kindly points out the works by Newley (1986), Weng, Carruthers & Perkins (1988), Belcher *et al.* (1990) suggesting the importance of pressure-gradient effects.) We tend to support that view but, again, it could well be that our conclusion above is correct anyway for any relevant model. The nominally small separation length

$\propto u_\tau^{\frac{1}{2}}$ (near the trailing edge) for instance appears to make sense in practical terms at finite Reynolds numbers. Typically $u_\tau$ is about 0.2, and so the separation length is about 0.45, i.e. separation could occur at approximately 55% chord. Further comments are presented in §5, including a note on computational evidence from Barnett & Carter (1986) (see also Neish 1988) tending to support the present conclusion, although firm experimental evidence seems to be lacking, as mentioned earlier. Remarks on and comparisons with the work of Sychev & Sychev (1980) and Sychev (1987), with whom there are fundamental differences, and Melnik (1989) (who suggests a two-parameter rather than the present one-parameter approach) and Deriat & Guiraud (1986), are also made in §5, with special note being made of the slip velocity induced within the turbulent boundary layer locally near separation according to the present theory.

## 2. Properties for turbulence parameter $Re^{\frac{1}{2}}\bar{T}$ of order unity

The theoretical study described below is on two-dimensional turbulence-modelled separation and follows on from that in Neish & Smith (1988) on turbulent wake flow. The aim is to understand in an asymptotic sense the nature of such separation when a representative and much-used turbulence model is taken throughout, for quasi-steady turbulent flow, and to judge whether the separation properties thus predicted are sensible or not.

The specific turbulence model chosen is the Cebeci–Smith one (see §1). With that model, and adopting here the artificial 'turbulence-level' parameter $T(\equiv Re^{\frac{1}{2}}\bar{T})$ introduced in §1, we address first the classical non-interactive boundary layer assumed on a thick airfoil, i.e. the composite scaled system consisting of

$$u = \partial\psi/\partial y, \quad v = -\partial\psi/\partial x, \tag{2.1a}$$

$$u\frac{\partial u}{\partial x}+v\frac{\partial u}{\partial y} = u_e u_e'+T\frac{\partial}{\partial y}\left(y^2B\left(\frac{\partial u}{\partial y}\right)^2\right)+\frac{\partial^2 u}{\partial y^2} \quad \text{for} \quad 0 \leqslant y < y_1(x), \tag{2.1b}$$

and

$$u = v = 0 \quad \text{at} \quad y = 0, \qquad u \to u_e(x) \quad \text{as} \quad y \to \infty. \tag{2.1c}$$

Here $u_e(x)$ is the prescribed edge velocity given by the assumed attached inviscid solution, $(\bar{y}, \bar{v}) = Re^{-\frac{1}{2}}(y, v)$ are scaled on $Re^{-\frac{1}{2}}$, as are $\bar{\delta}$ and the junction position, and, due to the $y$-scaling, the term $B$ is unity in the present setting (cf. §5), while the whole term $\propto T$ is replaced by a diffusive term in the usual way for $y > y_1(x)$; see (1.1*c*) above. The parameter $T$ is taken to be $O(1)$ at first here, although it is raised to its correct large size subsequently in §5. For the specific case of flow past a circular cylinder (figure 1), where in effect $u_e(x) \propto \sin \pi x$, $0 \leqslant x \leqslant 1$, computational solutions are described below, our particular interest being in the flow properties for increasing values of $T$.

To accommodate the stagnation point at the leading edge $x = 0+$ we put

$$\psi = x\tilde{\psi}; \quad u = x\tilde{u}; \quad \tau = x\tilde{\tau}; \quad u_e = x\tilde{u}_e; \quad \bar{\delta} = x\tilde{\delta} \tag{2.2}$$

(where $\tau \equiv \partial u/\partial y$ and $\bar{\delta}$ now incorporates an $Re^{-\frac{1}{2}}$ factor) and seek computational solutions for the tilde variables in $0 \leqslant x \leqslant 1$, where $x = 1$ defines the trailing edge. So the equations to be solved become

$$\tilde{u} = \frac{\partial\tilde{\psi}}{\partial y}, \quad \tilde{\tau} = \frac{\partial\tilde{u}}{\partial y}, \tag{2.3a, b}$$

$$x\left[\tilde{u}\frac{\partial\tilde{u}}{\partial x}-\tilde{\tau}\frac{\partial\tilde{\psi}}{\partial x}\right]+\tilde{u}^2-\tilde{\tau}\tilde{\psi} = \tilde{u}_e^2+x\tilde{u}_e\tilde{u}_e'+Tx\frac{\partial}{\partial y}[y^2\tilde{\tau}^2]+\frac{\partial\tilde{\tau}}{\partial y} \tag{2.3c}$$

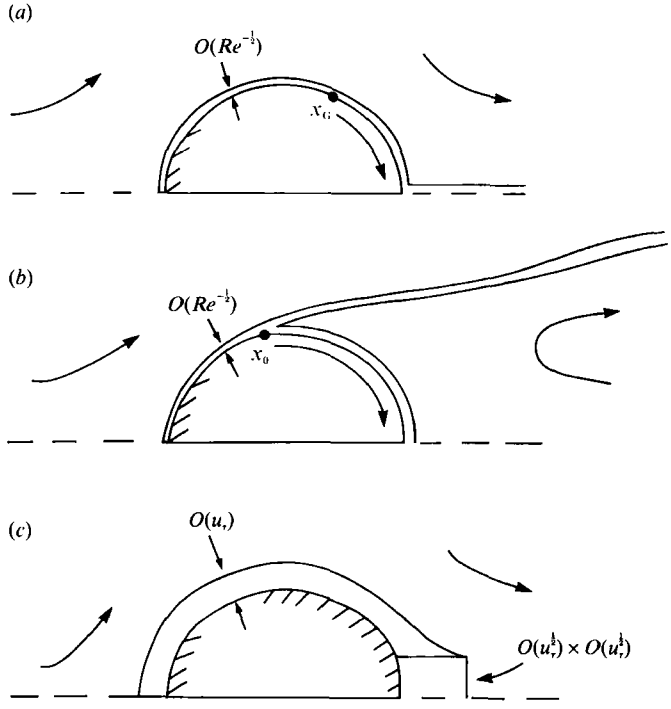


FIGURE 1. Schematic diagram concerning turbulent flow past a bluff body (circular cylinder). (*a*), (*b*) The effects of increasing the turbulence factor, starting from laminar flow, with (*a*) an attached boundary-layer assumption (§§2, 3), (*b*) separating flow (§4). The solid arrows indicate the movement of the breakdown position $x_G$ and the breakaway-separation position $x_0$ as the turbulence factor increases. (*c*) The resulting flow structure implied for fully turbulent flow, discussed in §5.

in the inner Cebeci–Smith form, the outer model having the turbulent-stress term replaced by $Tx(\partial/\partial y)[a_5\tilde{\delta}\tilde{\tau}]$. The boundary conditions here are

$$\tilde{\psi} = \tilde{u} = 0 \quad \text{at} \quad y = 0, \qquad \tilde{u} \to \tilde{u}_e \quad \text{as} \quad y \to \infty, \tag{2.3d, e}$$

for no slip at the surface, and for the outer-edge constraint respectively. Here $\tilde{u}_e = \sin \pi x/(\pi x)$ for $0 < x \leqslant 1$ with $\tilde{u}_e(0) = 1$ so that $u_e = x\tilde{u}_e$ has the required stagnation form at $x = 0, 1$.

Computational solutions of (2.3*a–e*) were obtained by means of a forward-marching Keller-box scheme, with locally uniform spacings $\Delta x, \Delta y$ in $x, y$ in adjoining parts of the computational domain $0 \leqslant x \leqslant 1$, $0 \leqslant y \leqslant y_E$, where $y_E$ is the upper edge. In the method, (2.3*a–c*) are replaced by

$$\tilde{u}^n_{j-1/2} = (\tilde{\psi}^n_j - \tilde{\psi}^n_{j-1})/\Delta y, \quad \tilde{\tau}^n_{j-1/2} = (\tilde{u}^n_j - \tilde{u}^n_{j-1})/\Delta y, \tag{2.4a, b}$$

$$x_{n-1/2}\left[\tilde{u}^{n-1/2}_{j-1/2}\left(\frac{u^n_{j-1/2} - \tilde{u}^{n-1}_{j-1/2}}{\Delta x}\right) - \tilde{\tau}^{n-1/2}_{j-1/2}\left(\frac{\tilde{\psi}^n_{j-1/2} - \tilde{\psi}^{n-1}_{j-1/2}}{\Delta x}\right)\right] + (\tilde{u}^2)^{n-1/2}_{j-1/2} - \tilde{\tau}^{n-1/2}_{j-1/2}\tilde{\psi}^{n-1/2}_{j-1/2}$$

$$= (\tilde{u}^2_e)^{n-1/2} + x_{n-1/2}\tilde{u}^{n-1/2}_e\left(\frac{\tilde{u}^n_e - \tilde{u}^{n-1}_e}{\Delta x}\right)$$

$$+ Tx_{n-1/2}\left[\frac{(y^2\tilde{\tau}^2)^{n-1/2}_j - (y^2\tilde{\tau}^2)^{n-1/2}_{j-1}}{\Delta y}\right] + \left(\frac{\tilde{\tau}^{n-1/2}_j - \tilde{\tau}^{n-1/2}_{j-1}}{\Delta y}\right) \tag{2.4c}$$

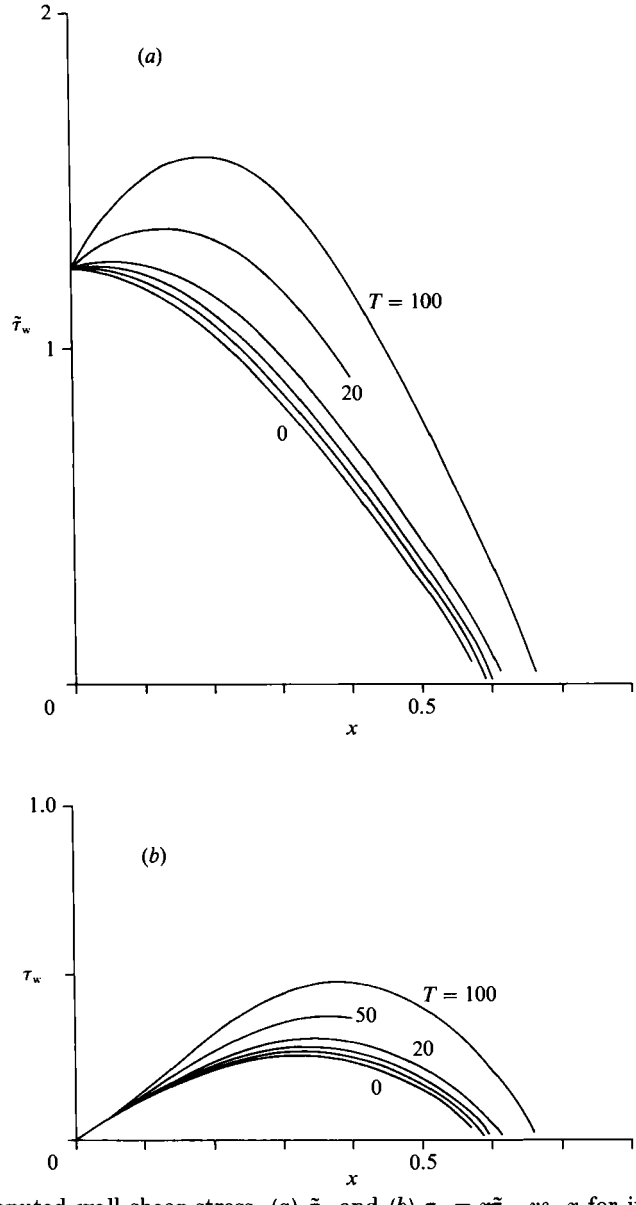


FIGURE 2. Computed wall shear stress, (*a*) $\tilde{\tau}_w$ and (*b*) $\tau_w = x\tilde{\tau}_w$, *vs.* $x$ for increasing values of $T$, showing the (slow) movement of the breakdown position $x_c$ towards the trailing edge at $x = 1$.

(and similarly for the outer model), the centring in (2.4*a*, *b*) being at $x_n, y_{j-1/2}$ as opposed to $x_{n-1/2}$, $y_{j-1/2}$ in (2.4*c*). Here in effect $x_n = (n-1)\Delta x$, $y_j = (j-1)\Delta y$ define the grid points in each part of the domain, $y_E = (J-1)\Delta y$, and affices $n$, $j$ refer to the function values at $x_n$, $y_j$, while $n-\frac{1}{2}$, $j-\frac{1}{2}$ refer to the averages of $n$, $n-1$ and $j, j-1$ values. The different parts involved correspond to different grid spacings $\Delta y$, finest near the surface ($j = 1$, $y = 0$), coarsest towards the upper edge, and medium in-between, and similarly for the $x$ spacing. Given the solution at the station $x = x_{n-1}$, the nonlinear equations (2.4*a–c*) along with the appropriate constraints at $j = 1$, $j = J$ enable the solution at the next station $x = x_n$ to be determined

iteratively to within a given tolerance. A Newton iterative approach, requiring inversion of a diagonally banded matrix to fix the Newton increments at each iteration, is used at that stage. A similar approach is taken at the front stagnation point $x = 0$, where the computations start, with (2.3*a–e*) yielding an ordinary differential problem then. Hence the scheme can be marched forward in $x$, with the solution at $x_{n-1}$ being used as the initial guess for the $x_n$ solution and so on. Further details of this and below are given by Neish (1988).

The typical grid employed has $\Delta x = 0.01, 0.02, 0.01$ in the $x$-intervals (0, 0.2), (0.2, 0.4), (0.4, 1) respectively, and $\Delta y = 0.01, 0.1, 0.5$ in the $y$-ranges (0, 0.5), (0.5, 5), (5, 10) in turn. The reasons for taking this type of distribution are based mainly on the multi-structured nature of the solution that is found to emerge at large $T$. Again, the effects on the results of increasing $y_E$ from 10, in the above grid, to 15, were found to be insignificant, and similar tests are described in the last reference above.

Results are presented in figures 2–7 for the wall shear stress $\tau_w$ versus $x$, $\tau_w$ versus $T$, $x_G$ versus $T$, velocity profiles, a close-up of the velocity profiles, and displacement thicknesses versus $x$, respectively. Here $x = x_G$ denotes the breakdown position of the boundary layer, at which the Goldstein (1948) singularity is encountered in the adverse pressure gradient over the rear half of the cylinder. It can be readily shown that Goldstein's theory and in particular its prediction of a square-root singularity, $\tau_w \propto (x_G - x)^{\frac{1}{2}}$ as $x \to x_G^-$, still apply to the turbulence-modelled equations (2.1) or (2.3). The dependence of $x_G$ on $T$, however, is of much interest.

In more detail, figure 2(*a*, *b*) presents plots of the wall shear stress $\tilde{\tau}_w$ and $\tau_w$ against $x$ for each value of $T$ considered. Each plot has a common value at $x = 0$ since there the flow is laminar and $T$ has no effect. The graphs clearly show increasing wall shear stress overall for increasing turbulence factor $T$, which is as expected from experimental evidence, and also the Goldstein point of zero wall shear stress moves towards the trailing edge, $x = 1$, for $T$ increasing, away from the point of laminar separation for $T = 0$. It is also interesting to note, on the other hand, that the zero-wall-shear-stress point moves only relatively slowly towards the trailing edge as the turbulence factor is increased to quite high levels. Edge effects hindered the calculations for values of $T$ larger than 100, well before the zero-wall-shear-stress point was reached in such cases.

Figure 3(*a*, *b*) shows plots of $\tau_w$ against $T$, at the stations $x = 0.3$ and 0.4 respectively, in order to check the analytical predictions in the following section. Accurate solutions for all values of $T$ are obtained at these stations, away from the stagnation point where tiny oscillations found in the results, due to the introduction of turbulence just after the leading edge, have most effect. Drawn on to the graphs are straight lines to demonstrate that the plots are close to linear, in anticipation of (3.7) below for large $T$.

Figure 4 presents the calculated zero-wall-shear-stress position $x_G$, against $T$, denoted by $\times$, and also the solid-line prediction for the position $x_G$ from §3 below. This indicates the slow movement of the zero-wall-shear-stress point towards the trailing edge, $x = 1$, as the turbulence factor is increased. This is discussed more later.

Further, figure 5(*a–j*) shows the velocity profiles for $T = 0$, 20, 100, at the points $x = 0.1, 0.2, 0.3, 0.4, 0.45, 0.5, 0.55, 0.6, 0.65, 0.66$. It is of interest to examine figure 5(*d*) for $x = 0.4$ since this shows distinctly the difference between the laminar and the turbulent boundary-layer profile, even though the boundary layer there is still under the influence of a favourable pressure gradient. Clearly the turbulent boundary layer is thicker in comparison, and in the majority of the flow it has a lower velocity, although near the wall the velocity is increased in comparison, within a small layer,

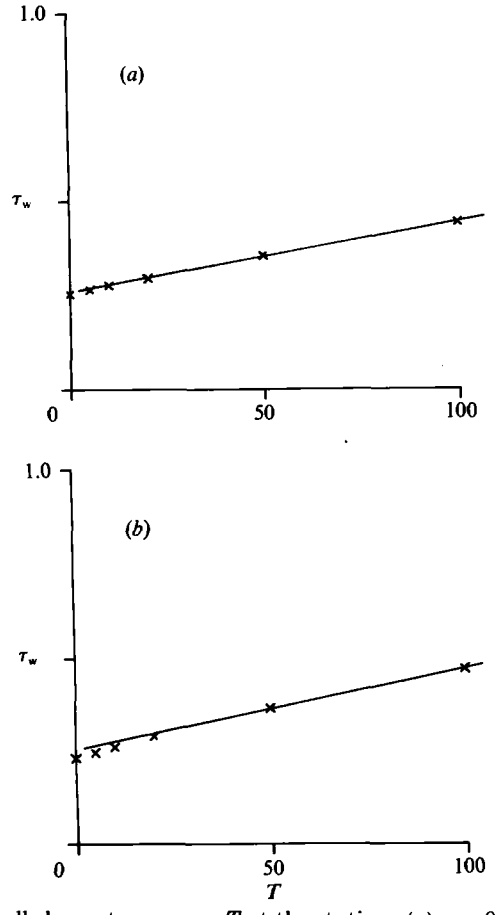


FIGURE 3. Computed wall shear stress $\tau_w$ *vs.* $T$ at the stations (*a*) $x = 0.3$ and (*b*) $x = 0.4$, shown by crosses. The solid straight lines indicate the near-linear behaviour of $\tau_w$ with $T$, for large $T$, in anticipation of (3.7).

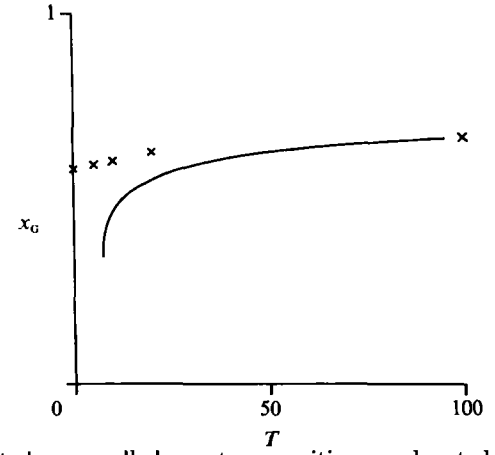


FIGURE 4. The calculated zero-wall-shear-stress position $x_G$, denoted by crosses, plotted against $T$, and the solid line prediction for $x_G$ from §3.

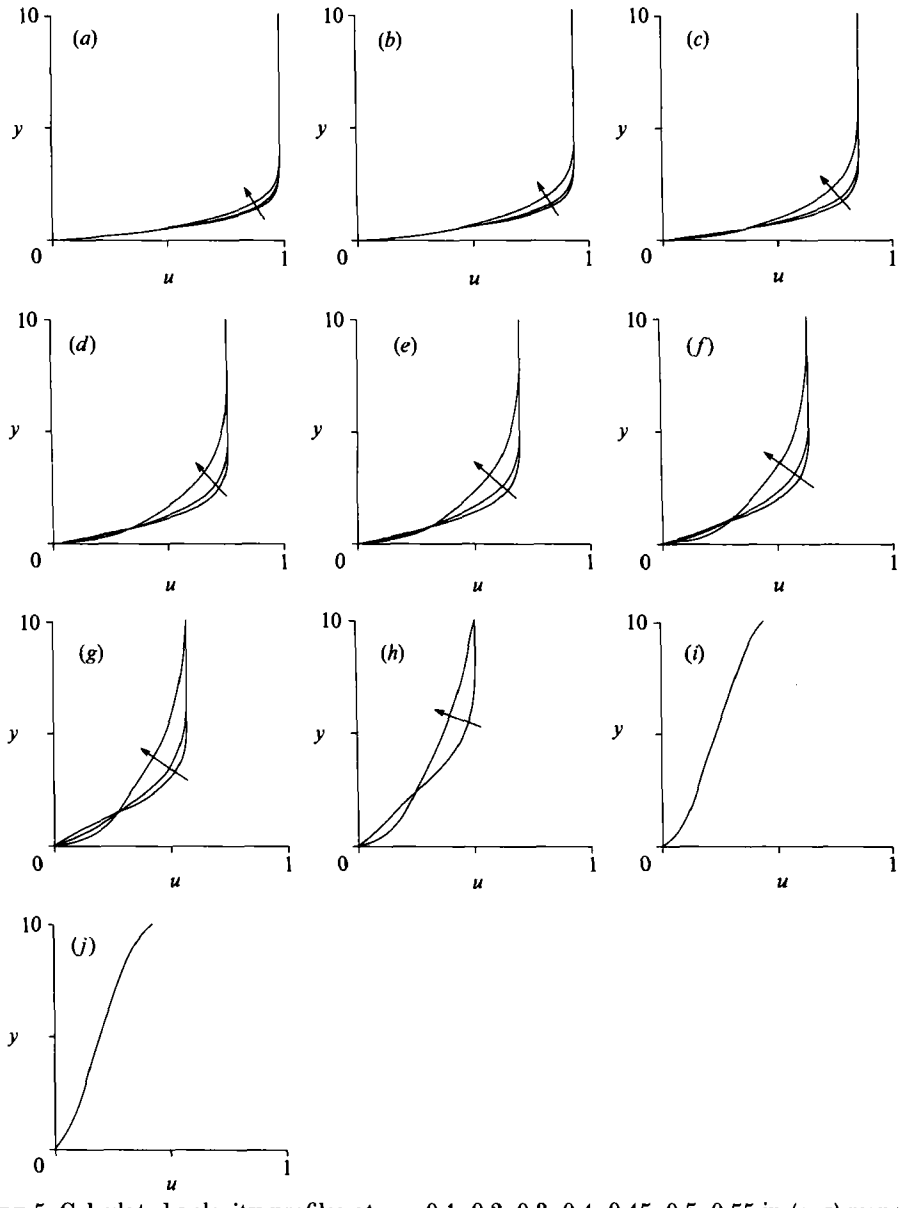


FIGURE 5. Calculated velocity profiles at $x = 0.1, 0.2, 0.3, 0.4, 0.45, 0.5, 0.55$ in $(a$–$g)$ respectively for $T = 0$, 20, 100; at $x = 0.6$ in $(h)$ for $T = 20$, 100 only; and at $x = 0.65$ and 0.66 in $(i)$ and $(j)$ respectively for $T = 100$ only. The arrows indicate increasing $T$. Note the possible resemblance to a Coles wake form near separation for large $T$ in $(i)$ and $(j)$.

giving increased shear stress at the wall. Figures 5(*a*)–5(*g*) clearly show a thickening boundary layer for $T = 0$, the laminar case, and 5(*g*) gives a typical profile approaching separation with a point of inflexion at about $y = 2.0$. Figures 5(*a*)–5(*h*) show the typically thicker turbulent boundary layer for $T = 20$, thickening greatly as separation nears in figure 5(*h*). The plots for $T = 100$ are in evident agreement with the expected trends as the turbulence factor is increased and have a possible resemblance to a Coles wake form near separation in figures 5(*i*) and 5(*j*) at $x = 0.65$ and 0.66 respectively. To emphasize the structure emerging near the wall at large $T$,

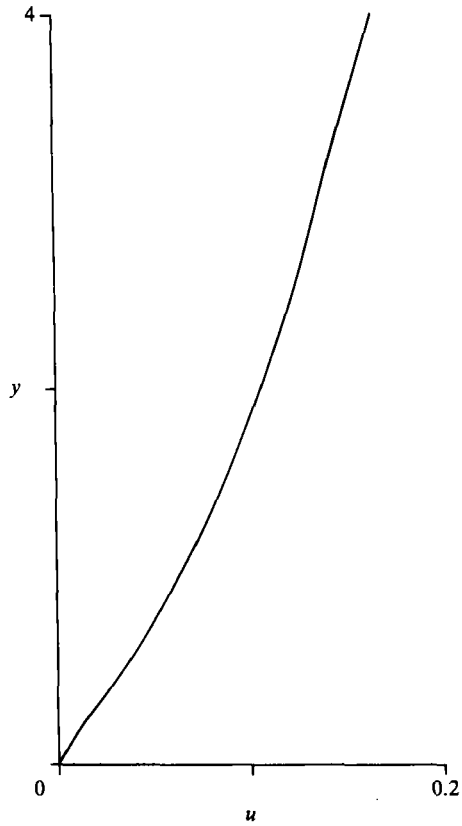


FIGURE 6. A magnification of the velocity profile in figure 5 (*j*) ($x = 0.66$, $T = 100$) for $0 \leqslant y \leqslant 4.0$, to emphasize the structure emerging near the wall for large $T$.

the profile is magnified in figure 6 for the $x = 0.66$ case with $T = 100$. We also note that for $x > 0.5$, the edge at $y_E = 10$ is having a clear effect on the outer part of the solution for the large-$T$ case and this may well be the cause of the computations for still larger values of $T$ failing long before the zero stress point is reached.

Finally, here, figure 7 gives plots of the displacement function $\bar{\delta} = u_e \delta$ (scaled with $Re^{-\frac{1}{2}}$) against $x$, for all values of $T$ in figure 7(*a*), and more clearly for $T = 0$, 20, 100 in figure 7(*b*).

## 3. Behaviour at large $Re^{\frac{1}{8}}\bar{T}$, and comparisons

Guided by the computational findings of §2, we turn now to the large-$T$ response of the turbulent boundary layer in (2.1), in order to approach the fully turbulent case (see §5). It is found below that the boundary layer takes on the classical turbulent two-tiered form rather than the original laminar form. The proposed large-$T$ structure is represented in figure 8(*a*), where the thickness scaling $\hat{\epsilon}$ is to be determined. The outer tier I of thickness $O(\hat{\epsilon})$ is found to have the usual turbulent stress–inertial balance of forces, to leading order, and the inner tier II of thickness of order $\tilde{\epsilon}$ (to be determined) has a turbulent–laminar stress balance to leading order.

In the outer tier I we set $y = \hat{\epsilon}\hat{y}$ and expand

$$u = u_e + \Delta \hat{u}_1 + \ldots, \tag{3.1}$$

where the unknown scale $\Delta \ll 1$ for large $T$. Then a turbulent–inertial balance is

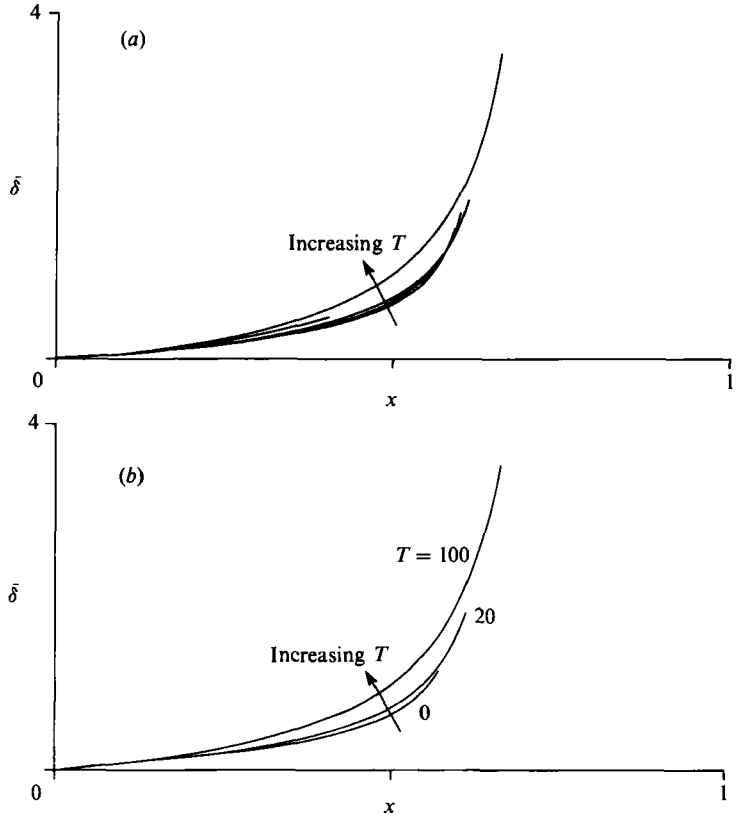


FIGURE 7. The computed displacement function $\bar{\delta} = u_e \delta$ plotted against $x$ for all values of $T$ in ($a$), and more clearly for $T = 0$, 20, 100 in ($b$).

regained, with, to leading order, the inviscid velocity–pressure relation $u_e u_e' = -p'$ holding, but at the next order the governing equations become

$$u_e \frac{\partial \hat{u}_1}{\partial x} + u_e' \hat{u}_1 - \hat{y} u_e' \frac{\partial \hat{u}_1}{\partial \hat{y}} = \begin{cases} \dfrac{\partial}{\partial \hat{y}}\left[\hat{y}^2 \left(\dfrac{\partial \hat{u}_1}{\partial \hat{y}}\right)^2\right] & \text{for} \quad 0 < \hat{y} < \hat{y}_1 \\ a_5 \bar{\delta} \dfrac{\partial^2 \hat{u}_1}{\partial \hat{y}^2} & \text{for} \quad \hat{y} > \hat{y}_1, \end{cases} \tag{3.2}$$

giving the inertial–turbulent stress balance, provided that $T\Delta = \hat{\epsilon}$. Here the continuity equation is used, $u_e' + \partial v / \partial \hat{y} = 0$, to give $v = -\hat{y} u_e'$ in (3.2). The boundary conditions are now

$$\hat{u}_1 \sim u_e[\ln \hat{y} + k_1(x)] \quad \text{as} \quad \hat{y} \to 0+, \qquad \hat{u}_1 \to 0 \quad \text{as} \quad \hat{y} \to \infty, \tag{3.3}$$

and $y_1 = \hat{\epsilon} \hat{y}_1$ defines the Cebeci–Smith junction point.

In the inner tier II, in contrast, $y = \tilde{\epsilon} \tilde{y}$ and a classical sublayer emerges, with $u = \Delta \tilde{u}_1 + \ldots$. So to leading order the laminar–turbulent stress-balance equation

$$0 = \frac{\partial}{\partial \tilde{y}}\left[\tilde{y}^2 \left(\frac{\partial \tilde{u}_1}{\partial \tilde{y}}\right)^2\right] + \frac{\partial^2 \tilde{u}_1}{\partial \tilde{y}^2} \tag{3.4}$$

is generated, provided that $T\Delta\tilde{\epsilon} = 1$. We also have the usual logarithmic matching condition and the no-slip wall condition,

$$\tilde{u}_1 \sim u_e[\ln \tilde{y} + k_2(x)] \quad \text{as} \quad \tilde{y} \to \infty, \qquad \tilde{u}_1 = 0 \quad \text{at} \quad \tilde{y} = 0. \tag{3.5}$$

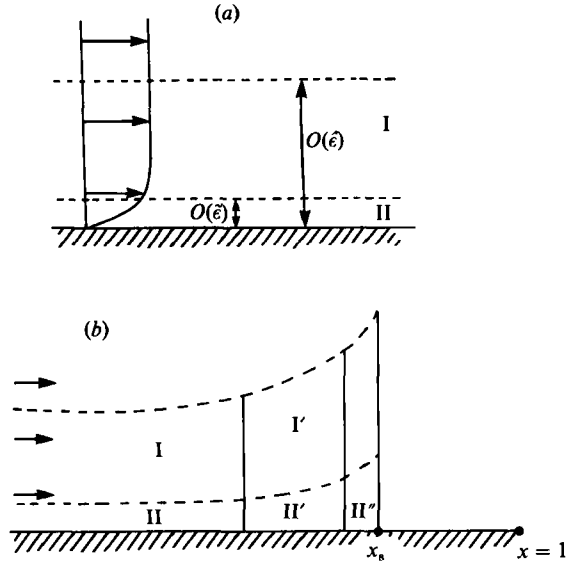


FIGURE 8. Schematic diagrams of (*a*) the undisturbed turbulent boundary layer structure for large $T$, with outer tier I thickness $O(\hat{\epsilon})$ having a turbulent stress–inertial balance of forces to leading order, and inner tier II thickness $O(\tilde{\epsilon})$ having a turbulent–laminar-stress balance to leading order; (*b*) the structures I′ and II′ implied by the stagnation point flow analysis, and the second new inner tier II″ where the boundary-layer equations hold and a Goldstein singularity is found to occur.

There are now two relations between the three unknowns $\hat{\epsilon}$, $\tilde{\epsilon}$, $\Delta$. The third relation follows from matching the velocity between the inner and outer tiers, which requires $\Delta \ln(\tilde{\epsilon}/T\Delta) = -1$. Hence we have

$$T = 2\hat{\epsilon}\ln\hat{\epsilon}, \quad \tilde{\epsilon} = \hat{\epsilon}^{-1}, \quad \Delta = \tfrac{1}{2}(\ln\hat{\epsilon})^{-1}, \tag{3.6a–c}$$

results which are consistent with the assumptions made above.

A major consequence of the *inner*-tier form is the near-linear prediction for the wall shear stress,

$$\tau \sim \frac{\hat{\epsilon}}{\ln\hat{\epsilon}} \quad \text{at large } T, \tag{3.7}$$

from (3.6*b*, *c*). This prediction is compared with the earlier described computations in figure 3.

Further, integration of the *outer*-tier equations (3.2) with respect to $\hat{y}$, from 0 to infinity, yields the result $(u_e^2\bar{\delta})' = u_e^3$ at each $x$, where the prime again stands for $\mathrm{d}/\mathrm{d}x$. Hence

$$u_e^2\bar{\delta} = \int_0^x u_e^3\,\mathrm{d}x, \tag{3.8a}$$

since $u_e^2\bar{\delta}$ is zero at the leading edge $x = 0$. In particular the integral term on the right-hand side of (3.8*a*) approaches a constant value, $E$ say, as $x \to 1-$ at the trailing edge/rear stagnation point for a finite body, which is of most concern here. So, for the flow past a circular cylinder, where we have $u_e \sim \lambda(1-x)$ as $x \to 1-$ with $\lambda$ a positive constant, the displacement function

$$\bar{\delta} \sim E\lambda^{-2}(1-x)^{-2} \tag{3.8b}$$

grows as expected as the trailing edge is approached. This result can now be used to guide the $x \to 1-$ behaviour of $\hat{u}_1$. By an order-of-magnitude argument

$\bar{\delta} \sim \hat{u}_1 \hat{y}$, giving $\hat{u}_1\ \hat{y} \sim |X|^{-2}$ as $X \equiv x-1 \to 0-$. The dominant inertial–turbulent balance in (3.2) also suggests the orders of magnitude $\hat{u}_1 \sim \hat{u}_1^2 \hat{y}^{-1} \sim \hat{u}_1 |X|^{-2} \hat{y}^{-2}$, so that $\hat{u}_1 \sim \hat{y} \sim |X|^{-1}$ approximately. In more accurate terms we must introduce a similarity variable $\eta$ for $|X| \to 0$ given by $\eta = \hat{y}|X|L$, so that $\hat{y} \sim |X|^{-1}L^{-1}$, where $L(|X|)$ is an unknown but slowly varying function of $|X|$ compared with powers of $|X|$. Then the velocity expands as

$$\hat{u}_1 = |X|^{-1} L f_0(\eta) + \ldots \tag{3.9a}$$

in order to preserve the above balance. The largest terms in the governing equations then are of order $|X|^{-1}L$ and cancel automatically. At the next order ($L'$) we obtain the equation(s)

$$-L'\lambda[f_0 + \eta f_0'] = \begin{cases} |X|^{-1}L^3 \dfrac{\partial}{\partial \eta}[\eta^2 f_0'^2] & \text{for} \quad 0 < \eta < \eta_1, \\ a_5 \delta_0 L^3 |X|^{-1} f_0'' & \text{for} \quad \eta > \eta_1, \end{cases} \tag{3.9b}$$

where $\delta_0 = E\lambda^{-2}$ and $\eta_1$ corresponds in the $\eta$-variable to the Cebeci–Smith junction $\hat{y}_1$ in the $\hat{y}$-variable. Thus there is an inertial–turbulent balance if $L' = |X|^{-1}L^3$, so that

$$L = (-2 \ln |X|)^{-\frac{1}{2}}, \tag{3.9c}$$

which satisfies the slowly varying assumption on $L$. For interest, the solution of the outer problem in (3.9$b$) is obtained by integrating once with respect to $\eta$ to give $-\lambda \eta f_0 = a_5 \delta_0 f_0'$, using the large$-\eta$ condition that $f_0$ vanishes faster than $\eta^{-1}$ (otherwise it is found that the velocity term $\hat{u}_1$ exhibits algebraic decay $\propto \hat{y}^{-1}$ at all $x$, including near the leading edge, which is unrealistic). Integrating once more yields the solution

$$f_0 = -A_0 \exp\left(-\frac{\lambda \eta^2}{2a_5 \delta_0}\right) \tag{3.10a}$$

which gives exponential decay for large $\eta$ as required. Similarly, for the inner problem, integrating once now gives $-\lambda \eta f_0 = \eta^2 f_0'^2$, since the constant of integration is zero, by continuity at the junction $\eta_1$. This yields the inner solution

$$f_0 = -(-\lambda^{\frac{1}{2}} \eta^{\frac{1}{2}} + A_1)^2 \tag{3.10b}$$

with continuity between (3.10$a, b$) at $\eta_1$. These solutions can be shown to confirm the small$-|X|$ behaviour of $\bar{\delta}$, in (3.8$b$).

Thus the small $|X|$ behaviours of $\hat{u}_1$ and $\hat{y}$ are predicted to be

$$\hat{u}_1 \sim |X|^{-1}(-2 \ln |X|)^{-\frac{1}{2}} f_0(\eta) + \ldots, \quad \hat{y} \sim |X|^{-1}(-2 \ln |X|)^{\frac{1}{2}}, \tag{3.11a, b}$$

as $|X| \to 0$. These responses can also be found by a transformation described by Neish (1988).

Closer to the trailing edge, however, the first two terms in the velocity expansion for the outer tier I become of equal magnitude. Balancing these terms as

$$|x-1| = |X| \to 0$$

gives $|X| \sim \Delta |X|^{-1}(-2 \ln |X|)^{-\frac{1}{2}}$. Recalling (3.6$c$), then, the balance occurs when $|X|$ is order $\gamma \ll 1$, say, where $\gamma$ is given by

$$-\gamma^4 \ln \gamma = \tfrac{1}{8}(\ln \epsilon)^{-2}. \tag{3.12}$$

This defines a new region where new physics governs the flow. It can be seen schematically in figure 8($b$), denoted by I′, where this region is extensive in the $y$-direction compared with the original classical outer tier I. The inner tier expands into a new region II′, also at distance $O(\gamma)$ from the rear stagnation point.

In region I′, the rescaling $x-1 = X = \gamma \bar{x}$ holds and $u = \gamma u^* + \ldots$, say, since

$u_e \sim \lambda|X|$ as $X \to 0$, the new expanded $y$-scale can be established from (3.11$b$), for then in I′, where $\bar{x}$ is of order 1, $y \sim \hat{\epsilon}\gamma^{-1}(-2\ln\gamma)^{\frac{1}{2}}$. Here $(-2\ln\gamma)^{\frac{1}{2}} = \Delta\gamma^{-2}$, and so we scale the new $y$-coordinate as $y = \hat{\epsilon}\Delta\gamma^{-2}y^*$, while by continuity $v = \hat{\epsilon}\Delta\gamma^{-2}v^* + \ldots$. With these scalings the governing equation for the flow I′ is nonlinear inertia/pressure-dominated,

$$u^*\frac{\partial u^*}{\partial \bar{x}} + v^*\frac{\partial u^*}{\partial y^*} = u_e^* u_e^{*\prime}\,[= \lambda^2|\bar{x}|] \tag{3.13$a$}$$

to leading order, together with continuity, and the significant point is that the velocity deficit is no longer small. Hence $u^{*2} - \lambda^2|\bar{x}|^2$ is constant along a streamline in I′. In particular along $y^* = 0^+$ we have a non-zero slip velocity $u_s^*$, where

$$u_s^{*2} - \lambda^2|\bar{x}|^2 = 2C, \tag{3.13$b$}$$

with the constant $C$ to be determined, since $y^* = 0^+$ is a streamline for this attached flow region. Breakdown occurs where the slip velocity vanishes and so, using (3.13$b$), we find a value for $\bar{x}$ at the breakdown point ($\bar{x}_s$ say in scaled coordinates, $x_s$ in $O(1)$ body-scale coordinates), i.e. $|\bar{x}_s| = (-2C/\lambda^2)^{\frac{1}{2}}$. The constant $C$ however can be found by matching upstream to the oncoming two-tiered structure (see earlier) where $|\bar{x}|$ is large. There the velocity has the form

$$u_1^* \sim \lambda|\bar{x}| + |\bar{x}|^{-1}G_0(\eta) + |\bar{x}|^{-3}G_1(\eta) + \ldots, \tag{3.14$a$}$$

where $\eta = y^*|\bar{x}|$. Substitution into (3.13$a$) gives nothing at orders $|\bar{x}|$ and $|\bar{x}|^{-1}$, since all terms there cancel, but at order $|\bar{x}|^{-3}$ gives an equation for $G_1(\eta)$ in terms of $G_0(\eta)$. Subsequently $G_0$ can be found by matching to the (earlier) oncoming classical solution as $(1-x) \to 0$. Also, then, on $y^* = 0$, we have from (3.14$a$) that $u_s^* = \lambda|\bar{x}| + |\bar{x}|^{-1}G_0(\eta) + \ldots$, which at $u_s^* = 0$ yields

$$|\bar{x}_s| = (-G_0(0)/\lambda)^{\frac{1}{2}}. \tag{3.14$b$}$$

This determines the constant $C = \frac{1}{2}\lambda G_0(0)$ in terms of the upstream solution. The boundary conditions for (3.13$a$) are then

$$u^* \sim u_s^* \quad \text{as} \quad y^* \to 0, \qquad u^* \to \lambda|\bar{x}| \quad \text{as} \quad y^* \to \infty.$$

The solution in region II′ can be found using the behaviours found earlier for II, where the turbulent–laminar stress balance in (3.4) gives $\tilde{u}_1\tilde{y} \sim 1$. Hence $\tilde{y}$ expands as $|X|^{-1}$, so that $\tilde{u}_1 \sim |X|$. Then within the new scale $X = \gamma\bar{x}$, the velocity expansion becomes $u = \Delta\gamma\tilde{\tilde{u}} + \ldots$ and the $y$-scaling and, by continuity, $v$-scaling are $y = \hat{\epsilon}^{-1}\gamma^{-1}\tilde{\tilde{y}}$, $v = \Delta\hat{\epsilon}^{-1}\gamma^{-1}\tilde{\tilde{v}} + \ldots$. The governing equation in II′ is therefore

$$\frac{\partial}{\partial\tilde{\tilde{y}}}\left[\tilde{\tilde{y}}^2\left(\frac{\partial\tilde{\tilde{u}}}{\partial\tilde{\tilde{y}}}\right)^2\right] + \frac{\partial^2\tilde{\tilde{u}}}{\partial\tilde{\tilde{y}}^2} = 0, \tag{3.15$a$}$$

so that the dominant physics in the inner tier remains unchanged. This also tends to confirm that the velocity-expansion breakdown in region I is the first physical change in the system, as the trailing edge is approached, and that no other new developments have been missed at an earlier stage further upstream. The boundary conditions in II′ are

$$\tilde{\tilde{u}} \sim u_s^*(\ln\tilde{\tilde{y}} + O(1)) \quad \text{as} \quad \tilde{\tilde{y}} \to \infty, \qquad \tilde{\tilde{u}} = 0 \quad \text{at} \quad \tilde{\tilde{y}} = 0. \tag{3.15$b$}$$

The flow solutions in regions I′, II′ match as required, and we note that a first integral of (3.15$a$), with (3.15$b$), gives

$$\tilde{\tilde{y}}^2\left(\frac{\partial\tilde{\tilde{u}}}{\partial\tilde{\tilde{y}}}\right)^2 + \frac{\partial\tilde{\tilde{u}}}{\partial\tilde{\tilde{y}}} = u_s^{*2}, \tag{3.15$c$}$$

from which the shear $\partial\tilde{\tilde{u}}/\partial\tilde{\tilde{y}}$ and hence the velocity $\tilde{\tilde{u}}$ can be found explicitly.

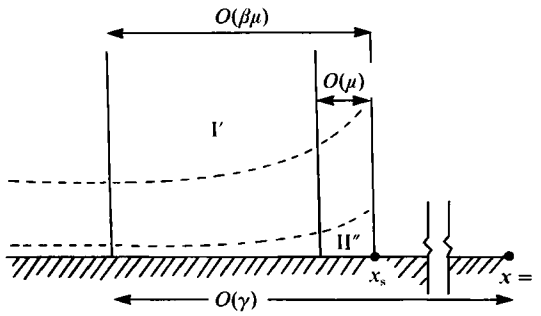


FIGURE 9. The construction used to determine the scales of inner tier II″ where $O(\beta\mu) \ll O(\gamma)$.

Returning to the solution in I′ as $\bar{x} \to \bar{x}_s$ from upstream, we have the property that

$$u_s^* \propto \lambda \xi^{\frac{1}{2}} \quad \text{as} \quad \xi \to 0, \tag{3.16}$$

where $\xi \equiv \bar{x}_s - \bar{x}$. Thus the solution has a square-root singularity (in distance) as breakdown is approached. This is different from the Goldstein singularity, however, which requires (see below) another region where the boundary-layer equations hold near the wall, denoted in figure 8 by II″. Thus turbulent breakdown is governed first by the outer tiers I, I′, which determine the position of the zero slip velocity and the form of the solution there. The inner tiers II and II′ serve only to modify the velocity profile near the wall, from the outer-tier slip to the no-slip condition at the wall. The inner tier II″, where the boundary-layer equations are found to hold, is here driven purely by the slip velocity induced in I′.

For region II″ we examine the variation of the quantities in II′, with $\xi$ small, under the influence of the slip velocity $u_s^*$. The velocity $\tilde{u}$ in II′ is driven by the large-$\tilde{y}$ condition in (3.15*b*), so that $\tilde{\tau} \equiv \partial\tilde{u}/\partial\tilde{y} \sim |\xi|^{\frac{1}{2}}\tilde{y}^{-1}$ for large $\tilde{y}$. The laminar–turbulent stress balance gives $\tilde{\tau}\tilde{y}^2 \sim 1$ in addition, and hence $\tilde{y} \sim \xi^{-\frac{1}{2}}$, $\tilde{u} \sim \xi^{\frac{1}{2}}$, $\tilde{\tau} \sim \xi$ as $\xi \to 0$. To determine the scales of II″ we make use of the construction shown in figure 9. The boundary-layer equations are assumed to hold in II″ which has $x$-scale $\mu$ (say) measured upstream from the zero velocity point, where $x = \mu\bar{x}$, and $\mu \ll \gamma$. The scale of the distance from the onset of the I′, II′ regions to the $u_s^* = 0$ point, $\bar{x}_s$, is taken to be $\beta\mu$, so that $X = \beta\mu\tilde{x}$ there and $\beta \gg 1$, $\beta\mu \ll \gamma$.

Then in the $\mu$-scale, $\xi$ is of order $\mu/\gamma$, since it is based on $\bar{x}$, and so at the $\beta\mu$-scale $\xi$ is of order $\beta\mu/\gamma$. Orders of magnitude for the quantities in zone II″ are thus given by $u \sim \Delta\gamma\beta^{-\frac{1}{2}}$, $y \sim \hat{\epsilon}\gamma^{-1}\beta^{\frac{1}{2}}$, based on the II′ scalings. Assuming that $\beta\mu \ll \gamma$, region II″ lies close to the $x \sim \gamma$ point. Then the pressure gradient in II″, based on the boundary-layer edge velocity $u_e$, is still of order $\gamma$ as in regions I′, II′; for the zero-slip-velocity point lies at a distance from $x = 1$ given by $\gamma - \beta\mu \sim \gamma$. Balancing inertial, turbulent, and viscous terms with this pressure gradient gives $\Delta^2\gamma^2\beta^{-1}\mu^{-1} \sim \hat{\epsilon}^2\Delta\gamma^3\beta^{-\frac{3}{2}} \sim \hat{\epsilon}^2\Delta\gamma^2\beta^{-\frac{3}{2}} \sim \gamma$, i.e.

$$\beta = \hat{\epsilon}^{\frac{4}{3}}\Delta^{\frac{2}{3}}\gamma^{\frac{4}{3}}, \quad \mu = \hat{\epsilon}^{-\frac{4}{3}}\Delta^{\frac{4}{3}}\gamma^{-\frac{1}{3}}. \tag{3.17}$$

This gives the boundary-layer equations in II″ where the Goldstein singularity occurs ($x = x_G$). The scalings are self-consistent in that $\mu$ is very small, $\beta\mu = \Delta^2\gamma$ is small compared with $\gamma$, and $\beta \gg 1$.

One prediction, then, is that the breakdown point, where the slip velocity reaches zero, and which coincides with the Goldstein breakdown position $x = x_G$ to leading order, is at a distance

$$\gamma(1 - \Delta^2) \tag{3.18}$$

from the rear stagnation point. Since the zero-slip-velocity point, indicating breakdown, lies at a distance from the rear stagnation point dependent logarithmically on $T$, its movement towards the stagnation point is very slow as $T$ is increased. In region II″ the scales are

$$|x-x_s| = \hat{\epsilon}^{-\frac{4}{3}} A^{\frac{4}{3}} \gamma^{-\frac{1}{3}} \bar{\bar{x}}, \quad y = \hat{\epsilon}^{-\frac{1}{3}} A^{\frac{1}{3}} \gamma^{-\frac{1}{3}} \bar{\bar{y}}, \quad u = \hat{\epsilon}^{-\frac{2}{3}} A^{\frac{2}{3}} \gamma^{\frac{1}{3}} \bar{\bar{u}} + \ldots \tag{3.19a}$$

we note, with the leading-order governing equation being

$$\bar{\bar{u}} \frac{\partial \bar{\bar{u}}}{\partial \bar{\bar{x}}} + \bar{\bar{v}} \frac{\partial \bar{\bar{u}}}{\partial \bar{\bar{y}}} = -\bar{\bar{u}}_e \bar{\bar{u}}'_e + \frac{\partial}{\partial \bar{\bar{y}}} \left[ \bar{\bar{y}}^2 \left( \frac{\partial \bar{\bar{u}}}{\partial \bar{\bar{y}}} \right)^2 \right] + \frac{\partial^2 \bar{\bar{u}}}{\partial \bar{\bar{y}}^2}, \tag{3.19b}$$

i.e. the full original system is recovered.

The principal extra comparison to be noted (see also earlier comparisons), between the numerical work of §2 and the present large-$T$ theory, is therefore for the breakdown position $x = x_G$; see figure 4, where the crosses denote numerical results and the solid line is the large-$T$ asymptotic prediction. For the smaller values of $T$ the calculated positions are rather remote from the theory, but for the larger values of $T$ the agreement is very close in terms of both the position and the speed at which the breakdown point moves towards the trailing edge. We observe the very slow rate at which this movement occurs; indeed, even for $T = 100$ the present theory predicts breakdown at approximately 0.665 (see also comments elsewhere concerning practical values).

## 4. Build-up from large-scale separated flow

An approach alternative to that in §§2, 3 is adopted here, with large-scale separation being assumed at the outset in the laminar-flow case at $T = 0$, for the motion past a thick airfoil or circular cylinder again. See figure 1. The effects of increasing $T$ from zero are then examined.

Extended Kirchoff free-streamline theory is taken to provide the underlying model at zero $T$, although similar conclusions hold for related models: see Smith (1979, 1985). On either side of the separation, at $x = x_0$ say, we therefore have

$$p \sim -\hat{\mu}(x_0 - x)^{\frac{1}{2}} \quad \text{as} \quad x \to x_0^-, \tag{4.1a}$$

$$S \sim \tfrac{2}{3}\hat{\mu}(x - x_0)^{\frac{3}{2}} \quad \text{as} \quad x \to x_0^+, \tag{4.1b}$$

with $p \equiv 0$ for $x > x_0$, and $\hat{\mu}$ a positive constant, where $p$, $S$ denote the surface/free-streamline pressure and the separated eddy thickness, respectively. The eddy's pressure and velocities are $o(1)$ throughout, while its length is $O(Re)$ and its maximum width is $O(Re^{\frac{1}{2}})$; see also the references above. Of most concern here however is the behaviour near the separation point, as the boundary layer breaks away. A triple-deck structure describes the separation process there, occurring through pressure–displacement interaction locally within the distance $|x-x_0| = O(Re^{-\frac{3}{8}}\lambda^{-\frac{5}{4}})$, where $\lambda$ is the $O(1)$ wall-shear-stress factor of the oncoming boundary layer. This requires $\hat{\mu}$ to be $O(Re^{-\frac{1}{16}})$ (Sychev 1972), corresponding to *smooth* separation, and as a result (4.1*b*) is adjusted to the form

$$S \sim \tfrac{2}{3}\alpha\lambda^{\frac{9}{8}} Re^{-\frac{1}{16}} (x - x_0)^{\frac{3}{2}} + \beta(x - x_0)^{\frac{5}{2}} + \ldots, \tag{4.2}$$

with $\alpha$, $\beta$ being $O(1)$ constants ($\alpha \approx 0.44$, Smith 1977). Solutions satisfying the viscous requirement (4.2) are described in the references above, where among other things it is found that the theory can work well in numerical terms at finite $Re$.

The main effect of introducing the turbulent influence $T$ into the overall motion is felt via the triple-deck local process of separation. In essence, increasing $T$ provokes

increasing wall-shear-stress factors $\lambda$ (see §§2, 3) and hence accentuates the first contribution in (4.2), as well as decreasing the triple-deck lengthscale. (This, we note, is akin to a decrease in the Reynolds number, in (4.2)). While $T$ is in the $O(1)$ range, however, $\lambda$ remains $O(1)$ also and so the smooth-separation criterion, represented by the term in $\beta$ in (4.2), remains undisturbed to leading order; this corresponds to the 55° separation position for Kirchhoff theory applied to the circular cylinder. To disturb the smooth-separation result, $\lambda$ must be increased to the order $Re^{\frac{1}{18}}$, as must $T$ approximately, in view of the theory in §3.

The same estimate for $T$, $\lambda$ results from comparing the triple-deck lateral extent ($O(Re^{-\frac{3}{8}}\lambda^{-\frac{5}{4}})$, equal to its streamwise extent) with the increasing turbulent boundary-layer thickness, which is $O(Re^{-\frac{1}{2}}T)$ from §3. The two are of equal order when

$$\lambda \sim T \sim Re^{\frac{1}{18}} \tag{4.3}$$

approximately, given (3.7) for the dependence of $\lambda$ on $T$ at large $T$.

It can now be verified that the laminar triple-deck structure around separation remains intact when (4.3) holds, despite the enlarged level of turbulence present. The three decks of the structure have $y$-scales of orders $Re^{-\frac{4}{9}}$, $Re^{-\frac{5}{9}}$, $Re^{-\frac{2}{3}}$ (upper, main, lower-deck respectively), in which the expressions

$$[u,v,p] = \begin{cases} [1,0,0]+O(Re^{-\frac{2}{9}}) & (4.4a) \\ [u_0,0,0]+O(Re^{-\frac{1}{9}},Re^{-\frac{2}{9}},Re^{-\frac{2}{9}}), & (4.4b) \\ [O(Re^{-\frac{1}{9}},Re^{-\frac{1}{3}},Re^{-\frac{2}{9}})] & (4.4c) \end{cases}$$

apply in turn, and $x \sim Re^{-\frac{4}{9}}$. These again yield the viscous–inviscid laminar separation problem of Smith (1977), since the extra turbulent-stress contributions remain small relative to the large $O(Re^{\frac{2}{9}})$ adverse pressure gradient and laminar-stress forces provoked locally during the triple-deck interaction. Further, although the upper deck's $y$-scale now coincides with the $O(Re^{-\frac{4}{9}})$ turbulent boundary-layer thickness, the typical potential-flow properties of the upper deck stay valid because of the small deficit of the oncoming turbulent velocity profile there: again see §3.

In consequence, the local laminar requirement (4.2) continues to hold even in the increasingly turbulent regime of (4.3); the factor $\lambda^{\frac{9}{8}}Re^{-\frac{1}{16}}$ is simply replaced by $\hat{\lambda}^{\frac{9}{8}}$, where $\hat{\lambda} \equiv Re^{-\frac{1}{16}}\lambda$ is $O(1)$. Thus the breakaway separation becomes *non-smooth* now, which is the major new feature, and in effect

$$\hat{\mu} = \alpha\hat{\lambda}^{\frac{9}{8}} \tag{4.5}$$

in (4.1*b*), with $\hat{\lambda} \propto \hat{T} \equiv Re^{-\frac{1}{16}}T$ of order unity. Increasing the turbulence factor $T$ then increases $\hat{\lambda}$ and hence $\hat{\mu}$, which drives the breakaway-separation position $x_0$ downstream along the surface, reducing the eddy length and width, as well as the $O(1)$ drag $c_D$. That trend continues until at a critical $O(1)$ value $\hat{\mu} = \hat{\mu}_c$ (where $\hat{T} = \hat{T}_c$, $\hat{\lambda} = \hat{\lambda}_c$) the drag $c_D$ tends to zero and $x_0 \to x_{0c}$ – say. This coincides with a *collapse* of the large-eddy structure, similar to that in Cheng & Smith (1982). For $\hat{\mu}$-values exceeding $\hat{\mu}_c$ (and $\hat{T} > \hat{T}_c$) the eddy length is smaller, of $o(1)$, with an eddy structure like that in the last reference or with a uniform-vorticity recirculating flow (see references above). In either case, as $\hat{\mu}$ continues to increase, the eddy size is almost certain to continue decreasing and the separation position to approach the trailing edge, essentially as in Cheng & Smith (1982), and $x_0 \to 1-$ as $\hat{\mu} \to \infty$, $\hat{T} \to \infty$, $\hat{\lambda} \to \infty$. So the same conclusion as in §3 is obtained, but from a different starting point; namely, that increasing the turbulence factor forces the separation towards the trailing edge, reaching the trailing edge asymptotically at large $\hat{T}$.

It is interesting also that formally as $T$ increases further, towards its fully turbulent value of order $Re^{\frac{1}{8}}$, the triple-deck structure condenses further. The next

distinct physical change to occur for large $T$ is when the lower tier of the triple deck and the turbulent-boundary-layer inner tier, of thickness $O(Re^{-\frac{1}{6}}T^{-1})$, become of equal magnitude. Since the lower deck has thickness of order $Re^{-\frac{5}{8}}\lambda^{-\frac{3}{4}}$, this occurs when $T \sim Re^{\frac{1}{2}}$, i.e. exactly in the fully turbulent case. At this scaling of the turbulence factor the upper and main decks of the triple-deck structure also collapse into the lower deck, and so we have a new single 'square' structure of dimensions $Re^{-1}$. Simultaneously the velocities $u$, $v$ and the pressure $p$ all become of $O(1)$, and so all the terms in the Navier–Stokes equations balance to leading order, i.e. we recover a small Navier–Stokes zone (see also Neish 1988). Since in this zone $x, y$ are of equal order, terms in the Reynolds-averaged Navier–Stokes equations originally neglected, i.e. the turbulence terms $T_{xx}$, $T_{yy}$ can also become important at leading order, requiring new types of turbulence modelling for these terms. Also in this zone the flow may turn through $O(1)$ angles, e.g. separate, requiring modification of the original turbulence models taken, since they are based on flow mainly in the $x$-direction parallel to the surface. Similar features have also been observed in experimental investigations by Thompson & Whitelaw (1985) and Simpson *et al.* (1977), who find strong flow rotation near the mean-flow separation, with normal stresses becoming important there.

A prominent feature of turbulent boundary-layer separation, then, seems to be that an $O(1)$ slope is required to provoke separation. In particular, the laminar flow past a wedge-shaped trailing edge can be studied in a fashion similar to the above. Figure 31 of Neish (1988) shows the flow configuration with a wedge having half-angle $\alpha$ and trailing edge at $x = 0$. The laminar theory (see e.g. Smith 1982) uses a triple-deck structure at the trailing edge with the lower deck having thickness of order $Re^{-\frac{5}{8}}\lambda^{-\frac{3}{4}}$, and length of order $Re^{-\frac{3}{8}}\lambda^{-\frac{1}{4}}$, so that the half-angle has order $Re^{-\frac{1}{4}}\lambda^{\frac{1}{2}}$ for separation to occur. Then as $T$ increases towards its fully turbulent value $Re^{\frac{1}{2}}$ separation is provoked, from the above, by an angle of increasing magnitude, until at $T = O(Re^{\frac{1}{2}})$ the angle $\alpha$ associated with fully turbulent boundary-layer separation becomes of order 1. This appears to be in qualitative agreement with some calculations (Barnett & Carter 1986, and see below) and experiments, and connects up with the theory in the following section.

## 5. Fully turbulent motion, and further discussion

The behaviour for fully turbulent motion ($\bar{T} = 1$), past a bluff body or thick airfoil, suggested by the work in §§2–4 is essentially that of attached non-interactive flow. Large-scale separation need not occur at all, at least according to the assumed turbulence model. Given the attached-flow inviscid solution outside, the two-tiered turbulent boundary layer is definitely able to remain attached right from the leading edge $x = 0$ to the onset of the trailing edge $x = 1$. Its small-deficit outer tier has thickness $O(u_\tau)$, the inner stress sublayer has thickness $O(u_\tau^{-1}Re^{-1})$, with the friction velocity $u_\tau$ being of order $(\ln Re)^{-1}$, and the resultant skin friction $\tau_W \propto u_e^2$ is bound to stay positive. Hence separation can be confined to the vicinity of the trailing edge $x = 1$; see also figure 1(*c*).

In more detail, and in line with the developments in §3, the two-tiered classical turbulent boundary layer for $0 \leqslant x < 1$ has the expansions

$$[u, \bar{v}/\epsilon] = [u_e(x), 0] + \epsilon[\hat{u}_1, \hat{v}_1] + \epsilon^2 \ln \epsilon[\hat{u}_{2L}, \hat{v}_{2L}] + \epsilon^2[\hat{u}_2, \hat{v}_2] + \dots, \tag{5.1a}$$

$$[u, \bar{v}] = [\epsilon\tilde{u}_1, Re^{-1}\tilde{v}_1] + \dots. \tag{5.1b}$$

in the outer and inner tiers respectively, with $\bar{y} = \epsilon\hat{y}$ and $\bar{y} = \epsilon^{-1}Re^{-1}\tilde{y}$ in turn. Here

$\epsilon \equiv (\ln Re)^{-1}$ is small, and $p = \hat{p}_0(x) + \epsilon^2 \hat{p}_2(x) + \ldots$, where $\hat{p}_0' = -u_e u_e'$. The governing equations and matching conditions for $\hat{u}_1$, $\tilde{u}_1$ are then effectively those in §3 (but with the term $B$ now differing from unity in the inner tier, due to the $\bar{y}$-scaling), the displacement thickness

$$\bar{\delta}(\equiv u_e \delta) = \int_0^\infty (u_e - u)\, d\bar{y} = \epsilon^2(\bar{\delta}_1 + \epsilon \ln \epsilon \bar{\delta}_{2L} + \epsilon \bar{\delta}_2 + \ldots) \tag{5.2}$$

also follows, and $u_\tau = O(\epsilon) + O(\epsilon^2 \ln \epsilon)$ can be worked out: see Neish & Smith (1988), Neish (1988). In particular, the skin friction is proportional to

$$(\partial \tilde{u}_1 / \partial \tilde{y})\,(x, 0) = u_e^2 \tag{5.3}$$

(see also Townsend 1976) and so remains positive throughout, while the main displacement-thickness contribution is given by

$$\bar{\delta}_1 = u_e^{-2} \int_0^x u_e^3\, dx; \tag{5.4}$$

see (3.8$a$). The result (5.3) stems from the integral version,

$$\hat{y}^2\{1 - \exp(-a_6 \tilde{y})\}^2 (\partial \tilde{u}_1 / \partial \tilde{y})^2 + (\partial \tilde{u}_1 / \partial \tilde{y}) = u_e^2,$$

of the momentum equation (3.4) in the inner tier, with the factor $B(\neq 1)$ incorporated and $\tilde{a}_6 = a_6 u_\tau \epsilon^{-1}$ is $O(1)$ for $0 \leqslant x < 1$.

Hence, on approach to the trailing edge, where $u_e \to 0+$ like $\lambda(1-x)$, (5.4) yields the growths

$$\bar{\delta}_1 \sim E/[\lambda^2 (1-x)^2], \quad \hat{y} \sim (1-x)^{-1} \tag{5.5}$$

in the displacement and the typical $\hat{y}$-scale (see (3.8$b$), (3.9$a$), and also the Appendix which shows among other things that the slip-velocity correction

$$k_1(x) \equiv (\hat{u}_1 - u_e \ln \hat{y})\ (\text{at } \hat{y} = 0)$$

grows like $(1-x)^{-1}$ as $x \to 1$. The corresponding externally induced pressure $\hat{p}_2$, given approximately by

$$-\frac{u_e}{\pi} \int_0^\infty \bar{\delta}_1'(\xi)\,(x-\xi)^{-1}\, d\xi,$$

therefore also grows, like $(1-x)^{-2}$. The typical boundary-layer slope, $\epsilon\, d\hat{y}/dx$, then becomes of order unity when $(1-x)$ is small, of order $\epsilon^{\frac{1}{2}}$ close to the trailing edge, and at the same stage the induced pressure $\epsilon^2 \hat{p}_2 \sim \epsilon^2 (1-x)^{-2}$ becomes comparable with the imposed pressure variation $\hat{p}_0 - \text{constant} \sim (1-x)^2$. So a new 'square' structure comes into operation when

$$x = 1 - O(\epsilon^{\frac{1}{2}}). \tag{5.6$a$}$$

An outer tier exists then, in which

$$[u, \bar{v}, p] = [\epsilon^{\frac{1}{2}} U, \epsilon^{\frac{1}{2}} V, \epsilon P] + \ldots, \quad \bar{y} = \epsilon^{\frac{1}{2}} \bar{Y}, \tag{5.6$b$}$$

and the governing equations are

$$U_{\bar{X}} + V_{\bar{Y}} = 0, \tag{5.7$a$}$$

$$UU_{\bar{X}} + VU_{\bar{Y}} = -P_{\bar{X}} + t_{\bar{X}}, \tag{5.7$b$}$$

$$UV_{\bar{X}} + VV_{\bar{Y}} = -P_{\bar{Y}} + t_{\bar{Y}}, \tag{5.7c}$$

expressing a nonlinear inertial/turbulent-stress balance. Here $x - 1 = \epsilon^{\frac{1}{2}} \bar{X}$. The solution of (5.7$a$–$c$) subject to the tangential-flow constraint $V = 0$ at $\bar{Y} = 0+$ yields a slip velocity

$$U \to U_s(\bar{X}), \quad V \to 0 \quad \text{as} \quad \bar{Y} \to 0+. \tag{5.8}$$

This is also implied by the analysis in §3, in particular by (3.11*a*) with (3.10b) and by (3.13*b*), and by the result for $k_1(x)$ quoted just after (5.5). A thinner sublayer is thereby provoked, bringing in the laminar stresses, to reduce the velocity to zero at the surface as in §3. Again see the Appendix. A match with the oncoming boundary-layer solution is possible at large negative $\bar{X}$, where the vorticity dependence is introduced (again as in §3), but then the slip velocity $U_s$ can be expected to reduce to zero at a finite value of $\bar{X}$, around which separation takes place. The smallest region involved there is a Navier-Stokes zone of $x$-, $\bar{y}$-dimensions approximately $O(Re^{-1})$ as described by Neish (1988). The local flow structure can then produce a closed-eddy flow for example, given that the local turbulent–laminar stress sublayers which are invoked still tend to stay attached as in (5.1)–(5.5). Thus although the theory remains tentative of course (see also later) the prediction

$$x_{\text{sep}} = 1 - O(u_7^{\frac{1}{2}}) \tag{5.9}$$

(approximately) is implied, for the separation position relative to the trailing edge at $x = 1$.

For comparison, a computational study of interest is by Barnett & Carter (1986) who use an interacting boundary-layer approach for turbulent flow past a NACA 0014 airfoil. Separation and eddy-closure positions are calculated at various Reynolds numbers, and it is found that both positions move towards the trailing edge as the Reynolds number increases, with attached flow being predicted beyond a Reynolds number of about $2 \times 10^6$. These trends agree with the present asymptotic theory. Further computations using various turbulence models are described by Arnold *et al.* (1989) and exhibit partly similar trends also.

Another comparison concerns the induced slip velocity in the lower reaches of the outer tier of the turbulent boundary layer. This slip velocity, i.e. $\hat{u}_s$ in §3 and $U_s$ in this section, comes into play non-trivially only within a small distance of separation, near the trailing edge, as the previously small $o(1)$ velocity deficit becomes an $O(1)$ deficit, in relative terms. This is in contrast with the suggestions of Sychev & Sychev (1980) and Sychev (1987) (see also Melnik 1989) who propose that such a slip velocity is produced within the chord-length boundary layer, unlike in (5.1*a*) ff. Their proposal, while interesting, seems questionable in our opinion mainly because a solution of the slip-affected outer-tier problem that arises in their work is simply $u \equiv u_e(x)$, as in (5.1*a*) and as implied by the computations and analysis of §§2, 3, and we believe that simple solution to be the general case unless extraneous forces impose a non-trivial slip velocity upstream. In addition the intermediate tier present in their suggestion is then unnecessary to the analysis, except near the trailing edge where the analogous tier is described in §3. Along with this, the present prediction of separation being focused near the trailing edge (see (5.9)), following the inverse-square displacement singularity of (5.5), is quite different from the previous theories above. We should also mention in passing here that the local inclusion of induced pressure-gradient effects, and the small-scale-separation zone governed by the Navier–Stokes equations, are addressed in more detail by Neish (1988); the small zone above yields, for weak disturbances, a Bessel-function dependence which is also found in a simultaneous study by Hunt *et al.* (1988). Likewise there are some links with theoretical work in progress on transition and turbulence dynamics, e.g. Smith, Doorly & Rothmayer (1990).

Turbulence modelling for separating boundary layers is in a relatively weak state, as remarked in §1, and that undoubtedly precludes forming a definite general conclusion on the separation position for instance. Nevertheless it is felt that the

present findings could well be correct for many separating flows and closure models. The separation distance of order $u_\tau^{\frac{1}{2}}$ in (5.9) for example makes sense in practical terms since $u_\tau^{\frac{1}{2}}$ is typically about 0.2–0.4 in the flow regimes of concern. Again, the present algebraic model taken reproduces the features found from more general models, e.g. in the references of the previous paragraph, and in Neish & Smith (1988) for wake flow. Finally, here, Deriat & Guiraud (1986) find an algebraic model to be essential for the correct description of the thin wall-layer flow and comment on its universality, even though adopting a $k$–$\epsilon$ model for the rest of the flow; again see also Neish (1988).

The present conclusion, for the Cebeci–Smith model and its like, is that large-scale separation need not occur, and if it does it is forced by the external flow for example reaching a stagnation point or altering abruptly. This is as opposed to the gentle alteration associated with laminar separation. The main lengthscales involved in the turbulent separation are then $O(u_\tau^{\frac{1}{2}})$, corresponding to the stagnation-point case. We observe that these scales could alter to $O(u_\tau)$ for instance in supersonic flow, notably for shock-wave/boundary-layer interaction, due to the suppressed upstream influence then (cf. the shrinking of the triple-deck structure described in §4). Further, the characteristic angle of separation is $O(1)$, since the streamwise and normal lengthscales are comparable, and hence the modelling of all the turbulent stress terms plays an essential role.

Helpful discussions with, and comments by, Professor T. C. Adamson, Dr M. Barnett, Mr S. P. Fiddes, Dr M. C. P. Firmin, Professor J. C. R. Hunt, Dr R. E. Melnik, Mr J. H. B. Smith, Professor J. D. A. Walker and Dr M. J. Werle are gratefully acknowledged, as are useful comments by the referees and the support of A.N. from the Department of Trade and Industry, through R. A. E. Farnborough.

## Appendix. Fully turbulent motion, matching and the induced slip velocity

In §5 we found a new 'square' structure for the flow close to the trailing edge, with streamwise lengthscale given by (5.6$a$). This structure comprises an outer tier, with scalings (5.6$b$) and governing equations (5.7$a$–$c$), yielding a slip velocity (5.8) and a thinner tier or sublayer required to reduce the velocity to zero at the surface. The following gives, in some more detail, the matching normally between the outer tier and the sublayer, and streamwise between these two tiers and the upstream classical two-tiered boundary-layer (cf. §3), resulting in a non-zero slip velocity in the solution for the outer tier.

Concerning first the classical outer tier, as the trailing edge is approached (5.6$a$, $b$), (5.7$a$–$c$) follow immediately in the new outer tier. The solution of (5.7$a$–$c$) then gives, near the surface,

$$U \sim F_{1L}(\bar{X}) \ln \bar{Y} + F_1(\bar{X}) \quad \text{as} \quad \bar{Y} \to 0+. \tag{A 1}$$

However, the signs are that $F_{1L}(\bar{X})$ is identically zero. For the small-$\hat{y}$ behaviour of the velocity in the upstream classical description, using (3.3), is

$$u \sim u_e + \epsilon[u_e \ln \hat{y} + k_1(x)] + \ldots \quad \text{as} \quad \hat{y} \to 0+, \tag{A 2}$$

which becomes in the new outer tier

$$u \sim \epsilon^{\frac{1}{3}}[U_e(\bar{X}) + \bar{k}_1(\bar{X})] + \epsilon^{\frac{3}{8}}[U_e(\bar{X}) \ln \bar{Y} + O(1)] + \ldots \quad \text{as} \quad \bar{Y} \to 0+, \tag{A 3}$$

where $u_e = \epsilon^{\frac{1}{3}} U_e$, $k_1 = \epsilon^{-\frac{1}{3}} \bar{k}_1$ (with $U_e, \bar{k}_1$ of order unity). The latter derives from consideration of (3.3), (5.5) and from the property that the velocity deficit $\hat{u}_1$ grows

like $(1-x)^{-1}$ typically as the trailing edge is approached; balancing of the scales implies that $k_1(x) \sim (1-x)^{-1}$ and this dominates (3.3) as $x \to 1$, i.e. the logarithmic part of the matching becomes *negligible*, being relegated to a higher-order effect, cf. the eradication of the logarithmic behaviour in Neish & Smith (1988), where a cusp-like velocity profile is produced instead. The leading-order term in (A 3) is a function of $\bar{X}$ only, and formally we may write it as $\epsilon^{\frac{1}{2}} U_s(\bar{X})$, defining the slip velocity for the solution to the new outer tier. Matching (A 1), (A 3) therefore to leading order is consistent with $F_{1L}(\bar{X}) \equiv O$, and $F_1(\bar{X}) \equiv U_s(\bar{X})$.

Secondly, regarding the classical inner tier, this behaves in a similar fashion to that found in §3. Thus, at the streamwise lengthscale of (5.6*a*), the tier expands to become a new inner tier in which

$$[u, \bar{v}, p] = [\epsilon^{\frac{3}{2}} \tilde{\tilde{u}}, Re^{-1} \epsilon^{-\frac{1}{2}} \tilde{\tilde{v}}, \epsilon P] + \ldots, \quad \bar{y} = Re^{-1} \epsilon^{-\frac{3}{2}} \tilde{\tilde{y}}, \tag{A 4}$$

giving at leading order a balance between the laminar and turbulent stresses,

$$\tilde{\tilde{u}}_{\tilde{\tilde{y}}} + \tilde{\tilde{y}}^2 \left( \frac{\partial \tilde{\tilde{u}}}{\partial \tilde{\tilde{y}}} \right)^2 = H_{1L}(\bar{X}), \tag{A 5}$$

after a normal integration, where the term $B$ is again unity due to the scaling (A 4). Solving we therefore find

$$\tilde{\tilde{u}} \sim H_{1L}(\bar{X})\, \tilde{\tilde{y}} \quad \text{as} \quad \tilde{\tilde{y}} \to 0+, \tag{A 6a}$$

$$\tilde{\tilde{u}} \sim H_{1L}^{\frac{1}{2}}(\bar{X}) \ln \tilde{\tilde{y}} + H_1(\bar{X}) \quad \text{as} \quad \tilde{\tilde{y}} \to \infty, \tag{A 6b}$$

so that the velocity does indeed reduce to zero at the surface. Matching with the classical inner tier upstream is straightforward. Writing (A 6*b*) in terms of the earlier $\bar{Y}$-coordinate yields

$$u \sim \epsilon^{\frac{1}{2}} H_{1L}^{\frac{1}{2}}(\bar{X}) + \epsilon^{\frac{3}{2}} [H_{1L}^{\frac{1}{2}}(\bar{X}) \ln \bar{Y} + O(1)] + \ldots \quad \text{as} \quad \bar{Y} \to 0+. \tag{A 7}$$

Matching with (A 1) again points to $F_{1L}(\bar{X})$ being zero, and $H_{1L}^{\frac{1}{2}}(\bar{X}) = U_s(\bar{X})$, the slip velocity. The fact that $U_s(\bar{X})$ is non-zero makes good sense in terms of (A 5)–(A 6*b*), and we note also that the skin friction now becomes proportional to $U_s^2(\bar{X})$, using (A 6*a*), rather than to $U_e^2$. Hence the skin friction stays positive until the new induced slip velocity tends to zero (which within the present lengthscale can occur ahead of a stagnation point in the flow outside the square structure).

## REFERENCES


ACHENBACH, E. 1971 Influence of surface roughness on the cross flow around a circular cylinder. *J. Fluid Mech.* **46**, 321.

ALBER, I. E. 1980 The turbulent wake of a thin flat plate. *AIAA J.* **18**, 1044.

ANDREOPOULOS, J. & BRADSHAW, P. 1980 Measurements of interacting turbulent shear layers in the near wake of a flat plate. *J. Fluid Mech.* **100**, 639.

BARNETT, M. & CARTER, J. E. 1986 An analysis of the crossover between local and massive separation on airfoils. *NASA Contractor Rep.* NAS1-16585.

BELCHER, S. E., WENG, W.-S., CARRUTHERS, D. J. & HUNT, J. C. R. 1991 The modelling of perturbed turbulent boundary layers. *Advances in Turbulence* 3 (ed. A. V. Johansson & P. H. Alfredsson), pp. 377–386. Springer.

BOGDONOFF, S. M. 1987 Observation of three-dimensional 'separation' in shock wave turbulent boundary layer iterations. In *Boundary-layer Separation* (ed. F. T. Smith & S. N. Brown). Springer.

BOGUCZ, E. A. & WALKER, J. D. A. 1987 The turbulent near wake at a sharp trailing edge. *J. Fluid Mech.* **196**, 555.

BRADSHAW, P. 1970 Prediction of the turbulent near-wake of a symmetrical airfoil. *AIAA Jl.* **8**, 1507.

BUSH, W. B. & FENDELL, F. E. 1972 Asymptotic analysis of turbulent channel and boundary-layer flow. *J. Fluid Mech.* **56**, 657.

CEBECI, T. & SMITH, A. M. O. 1974 *Analysis of Turbulent Boundary Layers.* Academic.

CEBECI, T., STEWARTSON, K. & WHITELAW, J. H. 1984 Calculation of two-dimensional flow past airfoils. In *Proc. 2nd Symp. on Numerical and Physical Aspects of Aerodynamic Flows* (ed. T. Cebeci). Springer.

CEBECI, T., THIELE, F., WILLIAMS, P. G. & STEWARTSON, K. 1979 On the calculation of symmetric wakes, I: Two-dimensional flows. *Numer. Heat Transfer* **2**, 35.

CHENG, H. K. & SMITH,. F. T. 1982 The influence of airfoil thickness and Reynolds number on separation. *Z. Angew. Math. Phys.* **33**, 151.

CHEVRAY, R. & KOVASZNAY, L. S. G. 1969 Turbulence measurements in the wake of a thin flat plate. *AIAA J.* **7**, 1641.

COLES, D. 1956 The law of the wake in the turbulent boundary layer. *J. Fluid Mech.* **1**, 191.

DEGREZ, G. & VANDROMME, D. 1985 Implicit Navier–Stokes calculations of transonic shock/turbulent boundary-layer interactions. In *Proc. IUTAM Symp. Turbulent Shear-Layer/Shock Wave Interactions* (ed. J. Délery). Springer.

DENGEL, P. & FERNHOLZ, H. H. 1990 An experimental investigation of an incompressible turbulent boundary layer in the vicinity of separation. *J. Fluid Mech.* **212**, 616.

DERIAT, E. & GUIRAUD, J.-P. 1986 On the asymptotic description of turbulent boundary layers. *Méc Theor. Appl.* Numero Special, p. 109.

ESCANDE, B. & CAMBIER, L. 1985 Turbulence modelling in transonic interactions. In *Proc. IUTAM Symp. Turbulent Shear-Layer/Shock Wave Interactions* (ed. J. Délery). Springer.

FENDELL, F. E. 1972 Singular perturbation and turbulent shear flow near walls. *J. Astronaut. Sci.* **20**, 129.

GERSTEN, K. 1987 Some contributions to asymptotic theory for turbulent flows. In *2nd Intl Symp. on Transport Phenomena in 'Turbulent Flows', Tokyo, Japan.*

GOLDSTEIN, S. 1948 On laminar boundary layer flow near a point of Separation. *Q. J. Mech. Appl. Maths.* **1**, 43.

HOFFMAN, G. D. & NY, B. S. H. 1978 Modelling of an asymptotic turbulent near wake using the interaction hypothesis. *AIAA J.* **16**, 193.

HUNT, J. C. R., LEIBOVICH, S. & RICHARDS, K. L. 1988 Turbulent shear flow over low hills. *Q. J. R. Met. Soc.* **114**, 1435.

HUNT, J. C. R. & RICHARDS, K. J. 1984 Stratified airflow over one or two hills. *Boundary-Layer Met.* **30**, 223.

INOUYE, M., MARVIN, S. G. & SHEAFFER, Y. S. 1972 Turbulent-wake calculations with an eddy viscosity model. *AIAA J.* **10**, 216.

JOHNSON, D. A. & KING, L. S. 1985 Transonic separated flow prediction based on a mathematically simple, nonequilibrium turbulence closure model. In *Proc. IUTAM Symp. Turbulent Shear-Layer/Shock-Wave Interactions* (ed. J. Délery). Springer.

LOCK, R. C. 1987 Velocity profiles for two-dimensional turbulent separated flows. In *Proc. IUTAM Symp. on Boundary-Layer Separation* (ed. F. T. Smith & S. N. Brown). Springer.

MELLOR, G. L. 1972 The large Reynolds number, asymptotic theory of turbulent boundary layers. *Intl J. Engng Sci.* **10**, 851.

MELNIK, R. E. 1980 Turbulent interactions on airfoils at transonic speeds – recent developments. *NATO AGARD Symp. Comput. of Viscous-Inviscid Flows, Colorado Springs, CO., Paper* 10.

MELNIK, R. E. 1987 A new asymptotic theory of turbulent boundary layers and the turbulent Goldstein problem. In *Proc. IUTAM Symp. Boundary-Layer Separation* (ed. F. T. Smith & S. N. Brown). Springer.

MELNIK, R. E. 1989 An asymptotic theory of turbulent separation. *Computers Fluids* **17**, 165.

MELNIK, R. E., CHOW, R. & MEAD, H. R. 1977 Theory of viscous transonic flow over airfoils at high Reynolds numbers. *AIAA paper* 77-680, presented at *10th Fluids & Plasma Dyn. Conf., Albuquerque, NM.*

MELNIK, R. E. & GROSSMAN, B. 1982 On the turbulent viscous-inviscid interaction at a wedge-shaped trailing edge. In *Proc. 1st Symp. Numerical and Physical Aspects of Aerodynamic Flows, Long Beach, CA* (ed. T. Cebeci). Springer.

NEISH, A. 1988 An asymptotic theory of two-dimensional turbulent boundary-layer separation and aligned flat plate–wake behaviour. Ph.D. thesis, University of London.

NEISH, A. & SMITH, F. T. 1988 The turbulent boundary layer and wake of an aligned flat plate. *J. Engng Maths.* **22**, 15.

NEWLEY, T. M. J. 1986 Turbulent airflow over hills. Ph.D. thesis, University of Cambridge.

PATRICK, W. P. 1985 Flowfield measurements in a separated and reattached flat plate turbulent boundary layer. *NASA Contractor Rep.* NAS3 – 22770.

POT, P. J. 1979 Measurements in a 2D wake and in a 2D wake merging into a boundary layer. *Natl. Aerosp. Lab. Rep.* NLR TR 70963, U, The Netherlands.

RAMAPRIAN, B. R., PATEL, V. C. & SASTRY, M. S. 1982 The symmetric turbulent wake of a flat plate. *AIAA J.* **20**, 1228.

SIMPSON, R. L., CHEW, Y.-T. & SHIVAPRASAD, B. G. 1981 The structure of a separating turbulent boundary layer. *J. Fluid Mech.* **113**, 23.

SIMPSON, R. L., STRICKLAND, J. H. & BARR, P. W. 1977 Features of a separating turbulent boundary layer in the vicinity of separation. *J. Fluid Mech.* **79**, 553.

SMITH, F. T. 1977 The laminar separation of an incompressible fluid streaming past a smooth surface. *Proc. R. Soc. Lond.* A **356**, 443.

SMITH, F. T. 1979 Laminar flow of an incompressible fluid past a bluff body: the separation, reattachment, eddy properties and drag. *J. Fluid Mech.* **92**, 171.

SMITH, F. T. 1982 On the high Reynolds number theory of laminar flows. *IMA J. Appl. Maths* **28**, 207.

SMITH, F. T. 1985 A structure for laminar flow past a bluff body at high Reynolds number. *J. Fluid Mech.* **155**, 175.

SMITH, F. T. 1986 Steady and unsteady boundary-layer separation. *Ann. Rev. Fluid Mech.* **18**, 197.

SMITH, F. T., DOORLY, D. J. & ROTHMAYER, A. P. 1990 On displacement-thickness, wall layers and mid-glow scales in turbulent boundary layers, and slugs of vorticity in channel and pipeflows. *Proc. Roy. Soc. Lond.* A **428**, 255.

STEWARTSON, K. 1969 On the flow near the trailing edge of a flat plate – II. *Mathematika* **16**, 106.

STRATFORD, B. S. 1959 The prediction of separation of the turbulent boundary layer. *J. Fluid Mech.* **5**, 1.

SYCHEV, V. V. 1972 On laminar separation. *Izv. Akad. Nauk. SSSR, Mekh. Zhid. Gaza* **3**, 47.

SYCHEV, V. V. 1987 On turbulent boundary layer separation. In *Proc. IUTAM Symp. Boundary-layer Separation* (ed. F. T. Smith & S. N. Brown). Springer.

SYCHEV, V. V. & SYCHEV, VIK. V. 1980 On turbulent separation . *Zh. Vyssh. Mat. Mekh. Fiz.* **20**, 1500.

SYKES, R. I. 1980 An asymptotic theory of incompressible turbulent boundary-flow over a small hump. *J. Fluid Mech.* **101**, 647.

THOMPSON, B. E. & WHITELAW, J. H. 1985 Characteristics of a trailing edge flow with turbulent boundary layer separation. *J. Fluid Mech.* **157**, 305.

TOWNSEND, A. A. 1976 *The Structure of Turbulent Shear Flow.* Cambridge University Press.

TRUPP, A. C., AZAD, R. S. & KASSAB, S. Z. 1986 In *Experiments in Fluids.* Springer.

WALKER, J. D. A. & ABBOTT, D. E. 1977 Implication of the structure of the viscous wall layer. In *Turbulence in Internal Flows.* (ed. S. N. B. Murthy), p. 131. Hemisphere.

WALKER, J. D. A. & SCHARNHORST, R. K. 1977 Solutions of the time dependent wall-layer flow in a turbulent boundary layer. In *Recent Advances in Engineering Science.* Lehigh University Press.

WALKER, J. D. A., SCHARNHORST, R. K. & WEIGAND, G. G. 1986 Wall layer models for the calculation of velocity and heat transfer in turbulent boundary layers. *AIAA Paper* 86-0213, *presented at 24th Aerospace Sciences Meeting, Reno, Nevada.*

WENG, W.-S., CARRUTHERS, D. J. & PERKINS, R. J. 1988 Proc. *2nd European Turbulence Conf.* (eds. H. H. Fernholtz & Fielder). Springer.